**Steel and Composite Structures**, *Vol. 31, No. 1 (2019) 99-112*
DOI: https://doi.org/10.12989/scs.2019.31.1.099


# Direct analysis of steel frames with asymmetrical semi-rigid joints

Jake L.Y. Chan *[1,2] and S.H. Lo [1]

[1] *Department of Civil Engineering, The University of Hong Kong, Pokfulam Road, Hong Kong, China*
[2] *Wo Lee Green Solutions Ltd., China*

(*Received July 28, 2018, Revised September 5, 2018, Accepted September 7, 2018*)

**Abstract.** Semi-rigid joints have been widely studied in literature in recent decades because they affect greatly the structural response of frames. In literature, the behavior of semi-rigid joints is commonly assumed to be identical under positive and negative moments which are obviously incorrect in many cases where joint details such as bolt arrangement or placement of haunch are vertically asymmetrical. This paper evaluates two common types of steel frames with asymmetrical beam-to-column joints by Direct Analysis allowing for plasticity. A refined design method of steel frames using a proposed simple forth order curved-quartic element with an integrated joint model allowing for asymmetrical geometric joint properties is presented. Furthermore, the ultimate behavior of six types of asymmetrical end-plate connections under positive and negative moment is examined by the Finite Element Method (FEM). The FEM results are further applied to the proposed design method with the curved-quartic element for Direct Analysis of two types of steel frames under dominant gravity or wind load. The ultimate frame behavior under the two different scenarios are examined with respect to their failure modes and considerably different structural performances of the frames were observed when compared with the identical frames designed with the traditional method where symmetrical joints characteristics were assumed. The finding of this research contributes to the design of steel frames as their asymmetrical beam-to-column joints lead to different frame behavior when under positive and negative moment and this aspect should be incorporated in the design and analysis of steel frames. This consideration of asymmetrical joint behavior is recommended to be highlighted in future design codes.

**Keywords:** bolted end-plate joint; plastic design; rigid/semi-rigid joint

## 1. Introduction

It has been well established that joint properties such as rotational stiffness and moment resistance play a significant role in the behaviour of unbraced steel structures but the common practice generally assumes joints as pinned or rigid. In advanced design using Direct Analysis, engineers commonly check frame stability and strength with allowance for joint properties.

The majority of design considers a joint to be most critical under gravity load and therefore more bolts may be provided at the tension zone of a joint rather than the compression zone. An asymmetrical joint flushed on the tension side and an extended end plate with rib stiffener on the compression side is a common joint detail for pitched roof portal frames and steel buildings. Any partial-strength asymmetrical joint of a frame under sequential loadings should account for possible moment reversal at critical joint locations rather than designed by assuming identical behaviour under positive or negative moments. However, asymmetrical performance of a joint is still yet to be implemented into the Direct Analysis method of design. For the case of under-estimation of strength and stiffness of joint, overstressing of certain members may occur. While overestimated stiffness and ductility of joints may invalidate the limit loads calculated by simplified asymmetric joint behaviour, it could cause unexpected deformation of structure and even collapse under design load at ultimate limit state.

In this paper, a parametric study on the performance of several asymmetric end plate joints under pure bending is first examined by finite elements and verified by 4 sets of experimental tests. Secondly, the overall structural performance of a pitched portal frame structure and a multi-storey structure utilizing the studied joints are analysed with the results obtained by both symmetrical and asymmetrical joint assumptions discussed.

## 2. Formulation of semi-rigid joint element model

Extensive numerical and experimental research has been conducted to investigate the nonlinear behaviour of the semi-rigid joints in the past two decades. For example, Chen and Kishi (1989) proposed a series of studies on semi-rigid joints. More recently, Valipour and Bradford (2013) carried out a 1-D frame element with flexible end joint that is capable of capturing the global response of multi-storey frames with matching accuracy to the displacement-based cubic hermit shape function. Also, Nguyen and Kim (2016) proposed an elastic-plastic beam-column element based on a displacement-based Newton-Rapson equlibrium iterative algorithm with consideration of flexibility in semi-rigid

*Corresponding author, Ph.D. Candidate,
E-mail: lokychan@hku.hk


http://www.techno-press.org/?journal=scs&subpage=6
ISSN: 1229-9367 (Print), 1598-6233 (Online)

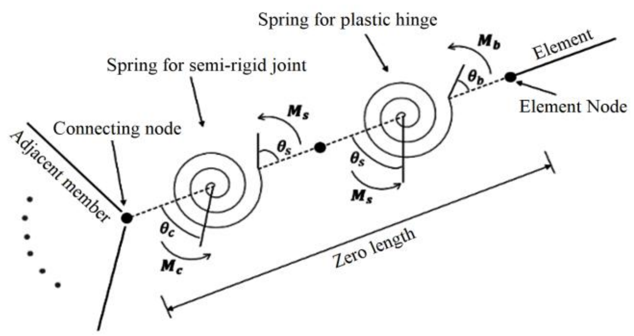


Fig. 1 Spring-in-series model for joint

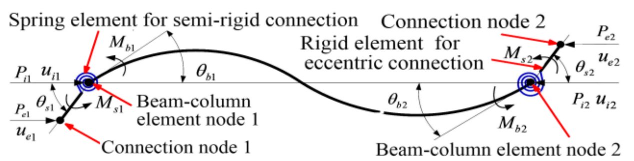


Fig. 2 Hybrid element with semi-rigid and plastic hinges at ends

joints. The semi-rigid behaviour is usually described by the moment versus joint rotation relations, while the joint stiffness changes according to the applied moments. Therefore, the instantaneous rotational stiffness of a semi-rigid joint can be calculated as section model (Figs. 1-2) during the incremental-iterative procedure requiring extensive computational time. As reported by Kwak and Kim (2002), by adopting the pre-generated M-P-Φ curves, this finite-element-based analysis method can be eliminated and dramatically improves design efficiency.

The basic element which can be used includes the most popular element namely the cubic Hermite element, the PEP element and the proposed fourth order element. Recognizing cubic element has inaccurate stiffness under high axial force, the upgraded fourth order element provides a sufficiently accurate displacement function for practical design. The element can be represented in Fig. 2 above.

### *2.1 Imperfect single columns with idealized boundary conditions*

An equation is assumed for the member imperfection as

$$v_{0y}(x) = v_{m0y}\left[1-(2x/L)\right] \tag{1a}$$

$$v_{0z}(x) = v_{m0z}\left[1-(2x/L)\right] \tag{1b}$$

in which $v_{m0y}$ and $v_{m0z}$ are the magnitudes of the imperfections at the mid-span of the element, $L$ is the element length and $x$ is the distance from the origin

The lateral deflection $v$ of the element is assumed to be the quartic shape function below

$$v(x) = a_0 + a_1x + a_2x^2 + a_3x^3 + a_4x^4 \tag{2}$$

where, $a_j$ is the coefficient in the shape function and $v$ is the lateral deflection. Boundary conditions are applied to the quartic shape function, as indicated in Figs. 1-2, which give

$$\text{When} \quad x = -\frac{1}{2}L, \quad v = 0 \tag{3}$$

$$\text{When} \quad x = +\frac{1}{2}L, \quad v = 0, \quad \frac{dv}{dx} = \theta_2 \tag{4}$$

$$\text{When} \quad x = 0, \quad v = \delta \tag{5}$$

in which, $L$ is the element length; $\theta_1$ & $\theta_2$ are the rotational angles at two ends and $\delta$ is the deflection at the mid-span, which is the internal degree-of-freedom to simulate the $P$-$\delta$ effect.

Making use of the energy principle, the secant and tangent stiffness matrices can be derived and used in conjunction with the Newton Raphson procedure for an efficient incremental-iterative non-linear analysis. This element allows for member imperfection as well as semi rigidity in end nodes. The present paper includes modelling of plastic hinges in the following section.

Non-linear material effect of plastic hinge is considered in this paper by the cross-section classification. Material yielding is accounted for by zero-length plastic hinges shown in Fig. 1 at one or both ends of each element. Here, two predefined section springs which are used to simulate plastic hinge and a new hybrid element is formulated. The internal degrees of freedom can be eliminated by a standard static condensation procedure, and therefore the bending equilibrium equations in an incremental form can be expressed as

$$\begin{bmatrix}\Delta M_{s1}\\ \Delta M_{s2}\end{bmatrix} = \begin{bmatrix} S_{s1}-S_{s1}^2(K_{22}+S_{s2})/\beta_s & S_{s1}S_{s2}K_{12}/\beta_s) \\ S_{s1}S_{s2}K_{21}/\beta_s) & S_{s2}-S_{s2}^2(K_{11}+S_{s1})/\beta_s \end{bmatrix} \begin{bmatrix}\Delta\theta_{s1}\\ \Delta\theta_{s2}\end{bmatrix} \tag{6}$$

With

$$\beta_s = \begin{vmatrix} K_{11}+S_{s1} & K_{12} \\ K_{21} & K_{22}+S_{s2} \end{vmatrix} > 0 \tag{7}$$

where $S_{si}$ is the stiffness of section spring, $\Delta M_{si}$ is the incremental nodal moment, $\Delta\theta_{si}$ is the incremental nodal rotations, $K_{ij}$ is the stiffness coefficients of the initially curved fourth order element.

To consider the progressive cross-section yielding, the section spring stiffness $S_s$ is simply defined below to approximate the inelastic behaviour of the steel members as

$$S_s = \frac{6EI}{L}\frac{|M_{pr}-M|}{|M-M_{er}|} \quad (M_{er} < M < M_{pr}) \tag{8}$$

where $EI$ is the flexural constant, $L$ is the member length, $M$ is bending moment due to external forces, and $M_{er}$ and $M_{pr}$ are the first yield and plastic moments respectively and they can be obtained as product of design strength and elastic and plastic moduli respectively.

In computer analysis, the section spring $S_s$ is taken as $10^{+10}$ $EI/L$ and $10^{-10}$ $EI/L$ for the elastic case (i.e., $M < M_{er}$)

and the plastic case (i.e., $M > M_{pr}$) respectively. The values are chosen because infinity is undefined numerically and $10^{+10}$ is the largest allowable value which has negligible difference in the calculated output when compared to a relatively smaller value that is above 25 $EI/L$. In case of a force point outside the full yield surface (i.e., $M > M_{pr}$), it should be moved back onto the surface to avoid the violation of plastic state by reducing the force and moment. The path of returning to yield surface is towards the origin of the force-moment surface.

The checking of plastic moment capacity $M$ in the presence of axial force can be obtained directly from the equation for section capacity check as

$$\frac{P}{P_y} + \frac{M}{M_p} = \emptyset \tag{9}$$

in which $P$ and $M$ are the applied axial force and moment, $P_y$ and $M_p$ are the axial force and moment capacities and $\phi$ is the section capacity factor and the section reaches full plasticity when $\phi$ is equal to 1.

With the formulation of element stiffness matrix, a nonlinear analysis can be carried out by a Newton-Raphson incremental-iterative procedure with constant load or by arc-length or minimum residual displacement constraints. Examples reported in this paper are conducted by the element and the standard nonlinear analysis procedure with the joint properties $S_s$ in Eq. (8) determined in the following sections. The proposed element seems to be most simple with allowance for plastic hinges and semi-rigid joints as well as member imperfection which are mandatory in contemporary design codes for Direct Analysis. Therefore, the theory reported in this paper can be directly applicable to practical problems of designing semi-rigid steel frames by the non-linear theory.

## 3. Review of end plate joint research

Extensive research work on static monotonic loading tests for different types of beam-column joints have been carried out in the past few decades. These experiments gave valuable data and insight for understanding the behaviour of various joint types and for modelling the joint component in the analysis.

Since the earliest studies of rotational stiffness of beam-column joints by Wilson and Moore (1917), numerous tests have been conducted to establish the relationship between moments and relative rotations of beam-column joints. Prior to 1950, riveted joints were tested by Young and Jackson (2011) and Rathbun (1936). In parallel with the interest in using high-strength bolts as structural fasteners, this joint type was tested by Bell *et al*. (1958). Subsequently, the behaviour of header plate joints was investigated in twenty tests by Sommer (1969).

Extended end-plate and flush end-plate joints have been used extensively since the late 1960's and extended end-plate joints are designed to transfer considerable moments from beams to columns. Flush end-plate and extended end-plate joints for more rigid connections were tested by Ostrander (1970) and Johnstone and Walpole (1981) respectively.

Davison *et al*. (1987) performed a series of tests on a variety of beam-to-column joints including the web-cleat, flange cleat, combined seating cleat and web cleats, flush end-plate and extended end-plate joints. An informative database of joint moment-rotation $M$-$\varphi c$ curves was established. Moore *et al*. (1993) carried out tests on five full-scale steel frames. The joints under the test included the flush end-plate joint, the extended end-plate joint and the flange cleat joint. Complete records of deformation of members and joints were reported. Liew *et al*. (1993) studied the qualities and limitations of the elastic-plastic method and the refined plastic-hinge method for direct frame design. Yu *et al*. (1998) reported differential behaviours of asymmetrical end-plate joints subjected to combined actions of member loads and lateral loads in the analysis of a sway frame. Kim *et al*. (2000) proposed a refined plastic-hinge analysis accounting for strain reversal due to sequential loading applied to structures. More recently, Li *et al*. (2014) investigated the 5 design parameters that influenced the joint performance most significantly by experiments and finite element models and found that the most important impact factors are the T-stub connecting parts and the number of bolts. Daryan *et al*. (2012) examined the time history response of semi rigid frame with angle bolted joint under lateral loadings. Rafiee *et al*. (2013) derived an optimum design algorithm capable of identifying the best design solution for steel frames utilizing a selection of semi-rigid joints. Sagiroglu and Aydin (2013) derived the Frye-Morris polynomial model for nonlinear behaviour of double web angle joints and compared the performance of unbraced rigid and semi-rigid structures. Liu *et al*. (2016b) studied the contribution of floor stiffness for steel structures with semi rigid end plate joint. Bai *et al*. (2016) evaluated the failure probability of steel frame under: (1) linear semi-rigid; (2) nonlinear semi rigid; and (3) nominally pinned joints by the monte-carlo simulation and found that joint rigidity have strong impact on the structural integrity of steel structures.

Majority of these studies assumes symmetrical properties for joints. For symmetrical joints, the stiffness is theoretically identical but for most joints with asymmetrical geometry, the stiffness for joint is under sagging moment is understandably higher due to better stress distribution between the bolts at tension zone and at the end plate. As a result, the member and frame behaviour under moment reversal may be significantly different for symmetrical joints. Asymmetrical cap plate and extended end plate joints under predominant positive bending were tested by Nassani *et al*. (2017) and but no Load Case leading to moment reversal is investigated. This paper is aimed to investigate the non-linear behaviour of steel frames with asymmetrical joints under the influence of realistic load cases leading to moment reversal.

Eurocode 3 (2005) proposes the limit state approach of checking strength of individual joint components based on common design variables such as thickness of end plate, column flange, as well as the diameter of bolt. It was popular to follow the AISC (2010) guidelines that lead to design of a fairly thick plate due to the design assumption of column flange and end plate being perfectly elastic and relatively stiff. However, with the introduction of the Tee stub model, the prying force of bolt can be determined and a more economical design can be resulted. The works of Sagiroglu and Aydin (2015) has demonstrated a structural weight reduction of up to 9% can be achieved for multi-storey frames adopting semi-rigid joints compared to using fully rigid joints.

The yield-line theory, which establishes the relationship between yielding pattern and the strength of joint components, is also used in Eurocode 3 (2005). The design guides by SCI (2014) encompasses a range of common yield-line patterns such as circular or grouped, and accommodating common bolted joint types such as flushed end plate joint and extended end plate joint with and without stiffener ribs. In general, engineers favour bolt resistance to be significantly larger than the strength of other components in the joint in order to ensure ductility and rotational capacity, which results in a less stiff structure in exchange for a more gradual or prolonged progressive collapse.

One of the few coverages in design for moment reversal in joints is found in AISC (2010) which is related to checking of welds in compression flange when under tension due to moment reversal. However, no literature is found about its influence on global stability of steel frames. This paper fills this gap of studying frames with allowance for the asymmetrical joint responses.

## 4. Finite element model (FEM) and experimental verification

This paper first validated the accuracy of the FEM by full-scale test of an extended end-plate joint (Fig. 3 and Table 1). A comparison of the deformation characteristic after yielding is presented in Fig. 4. Similar to most previous finite element analysis and studies, reliability of FEM in joint modelling is confirmed and accurate results were obtained and reported. Briefly speaking for the present studies, the FEM package ABAQUS (2014) was used to evaluate the structural performance of asymmetrical bolted joints under pure bending. Material yielding is captured by adopting three-dimensional eight-node linear brick elements C3D8 for modelling of all joint components. The contact

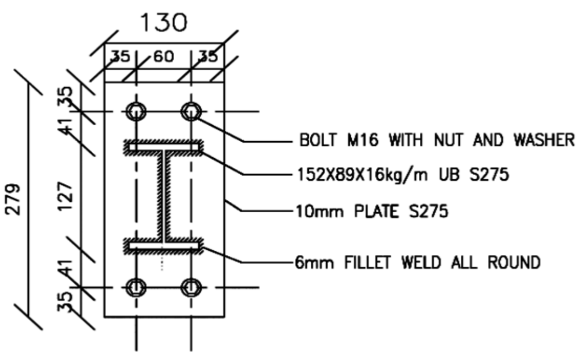


Fig. 3 Joint configuration

Table 1 Joint configuration

| | | |
|---|---|---|
| All | Steel grade | 275 N/mm$^2$ |
| Beam | Section | 152×89×16 kg/m UB |
| | Span | 1 m |
| Column | Section | 152×152×23 kg/m UC |
| End plate | Thickness | 10 mm |
| | Width | 130 mm |
| | Height | 279 mm |
| Bolts | Vertical distance | 209 mm |
| | Horizontal distance | 60 mm |
| | Grade | Gr 8.8 |
| | Size | 16 mm diameter |

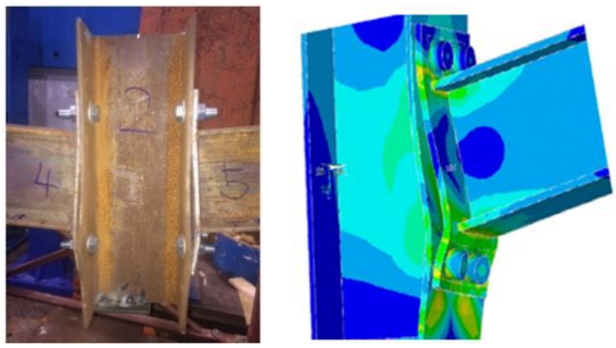

Fig. 4 Tested specimen and strain diagram (FEM)

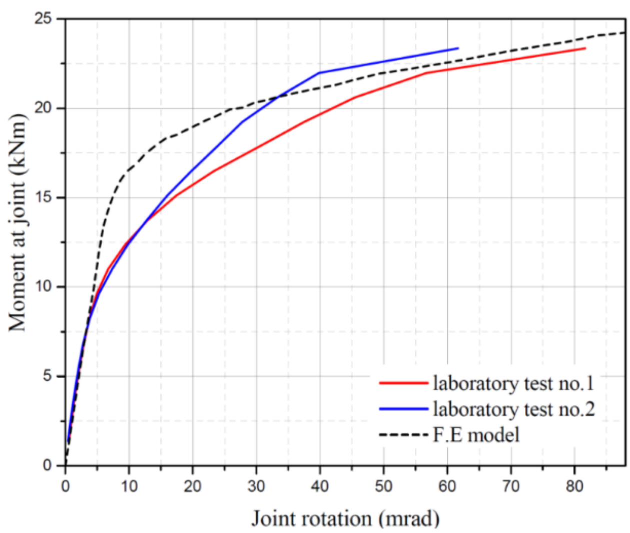


Fig. 5 Moment versus joint rotation

between a bolt nut and an endplate is established by applying a designated preload along the bolt shank and then fixing the bolt length in the remaining analysis. The material properties adopted in the FEM are obtained from coupon tests for various key locations of the sample specimens. The Newton Rapson analysis with constant displacement control is adopted for iterative convergence at the second half of the numerical simulation. By indication

Table 2 Comparison of analytical results for joint bending resistance, rotational stiffness, and rotational capacity

| Specimen | Moment resistance | Initial rotational stiffness | Rotational capacity | Failure mode |
|---|---|---|---|---|
| | $M_{j,Rd}$ (KN.m) | $S_{j,ini}$ (MN.m/rad) | $\Phi_c$ (mrad) | |
| Experiment No. 1 | 21.9 | 2.6 | 56.5 | End plate yielding |
| Experiment No. 2 | 22.1 | 2.6 | 40.1 | End plate yielding |
| Finite element analysis | 21.4 | 2.4 | 36 | End plate yielding |

of maximum strain value of strain gauge attached to the end plate, it is noted that the initial yielding for both the experimental test and the FEM occurred at the end plate location adjacent to the beam bottom flange. The initial rotational stiffness and ultimate moment resistance are also in good agreement as shown in Table 2. However, the *M-θ* graph comparison in Fig. 5 shows that a lower stiffness is observed for both of the experimental results at mid rotation range prior to first yielding, which can be explained by its lack of fit and subsequent slip between components such as gaps between bolts and bolt holes, gradually displace under higher load applied to the specimens.

## 5. Design consideration of joint types

The relationship between the number of tension bolt row for eaves joint under positive moment and the joint performance was carried out by parametric studies using FEM. The specimens were designed to withstand a design moment of 20 kNm according to the limit state of the gable frames (Fig. 6) studied in this paper. Six joint models were designed for ductile failure. Further explanation will be given on the FEM results.

The two distinct types of asymmetrical joints in the gable frame (Fig. 6) are eaves joint (Type C model) (Figs. 7-9) and apex joint (Type D model) (Figs. 10-12).

Design parameters of the six joints are shown in Tables 3 which describe the number of tension bolts and shear bolts under gravity load case. Material properties for the FEM are shown in Table 4. The boundary conditions and

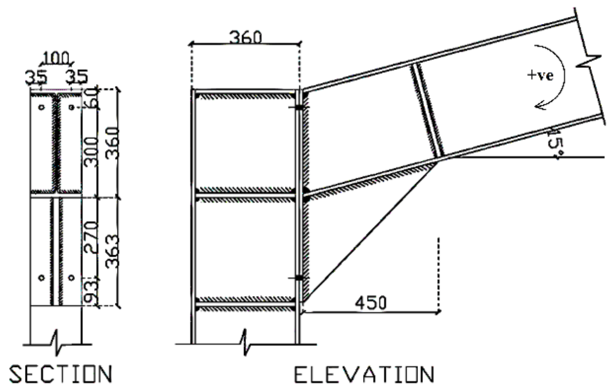


Fig. 7 Type C1 joint (contain 1 row of tension bolts when under +ve moment)

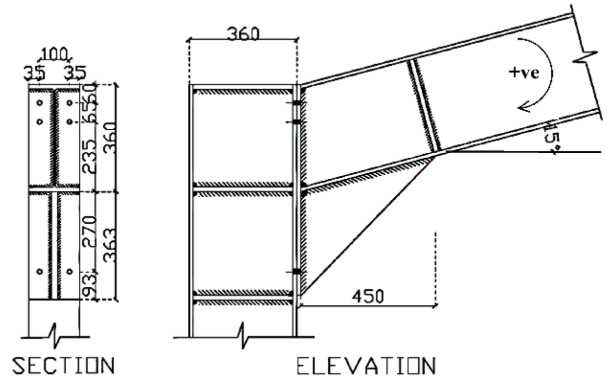


Fig. 8 Type C2 joint (contain 2 row of tension bolts when under +ve moment)

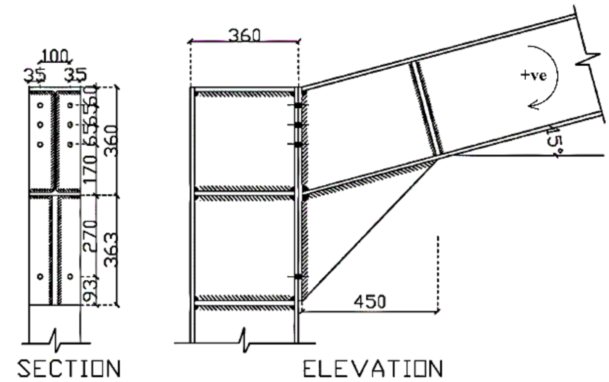


Fig. 9 Type C3 joint (contain 3 rows of tension bolts when under +ve moment)

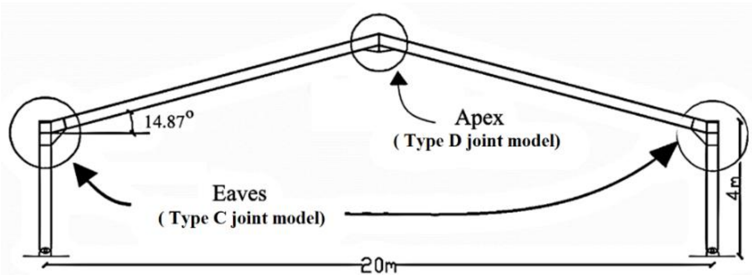


Fig. 6 Vogel gable frame for our current study

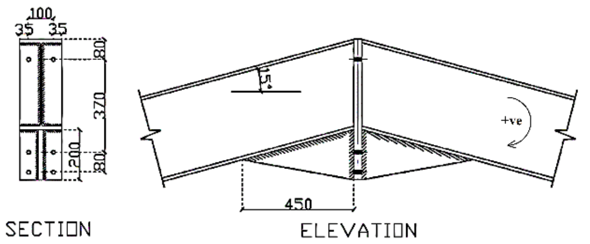


Fig. 10 Type D1 joint (contain 1 row of tension bolts when under +ve moment)

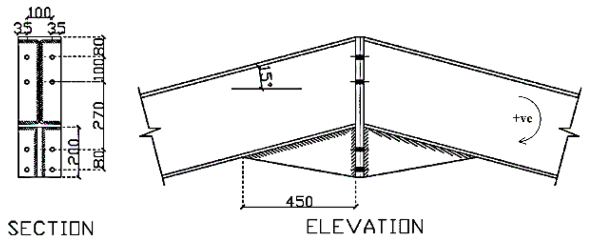


Fig. 11 Type D2 joint (contain 2 rows of tension bolts when under +ve moment)

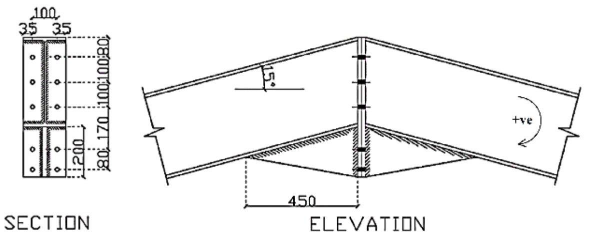


Fig. 12 Type D3 joint (contain 3 rows of tension bolts when under +ve moment)

Table 4 Material properties from Vogel (1985)

| Material | Yield strength (MPa) | Tensile strength (MPa) |
|---|---|---|
| Beam | 235 | 360 |
| Column | 235 | 360 |

*Notes: Elastic modulus is 206000 Mpa and bolt pretension force is 185 kN

the method of loading are described in Figs. 13 and 14. It can be assumed rationally that under gravity load case, the top bolt rows of a Type C joint are principally stressed by bending while the bottom bolt rows are by shear. For a type D joint, the bottom bolt rows are principally stressed by bending while the top bolt rows are by shear.

The contribution of shear and axial force towards the failure of the Type C and Type D joints is found to be less than 5% of the member section capacity and hence these joints are considered as being stressed principally by bending.

## 6. Results and discussions

Joint asymmetry in the form of bolt group arrangement and end-plate rib stiffener is found to have significant influence on the performance of the studied joints in this paper.

### *6.1 Governing failure modes*

The strain distribution and deformation at first yielding for type C joints and type D joints are shown in Figs. 16 to 19.

Table 3 Design parameters of joints under Load Case1 (Gravity load only)

| Joint No. | Joint location | Web stiffener thickness (mm) | End-plate thickness (mm) | Number of tension bolt row | Number of shear bolt row |
|---|---|---|---|---|---|
| C1 | Eaves | 15 | 13 | 1 | 1 |
| C2 | Eaves | 15 | 13 | 2 | 1 |
| C3 | Eaves | 15 | 13 | 3 | 1 |
| D1 | Apex | N/A | 16 | 1 | 2 |
| D2 | Apex | N/A | 16 | 2 | 2 |
| D3 | Apex | N/A | 16 | 3 | 2 |

*Notes: All member size is IPE360, All bolt diameter is 24 mm and all beam web rib stiffener haunch thickness is 20 mm. Tension bolt is principally stressed in tension by bending moment at the joint while shear bolt is principally stressed by shear force under the gravity load case

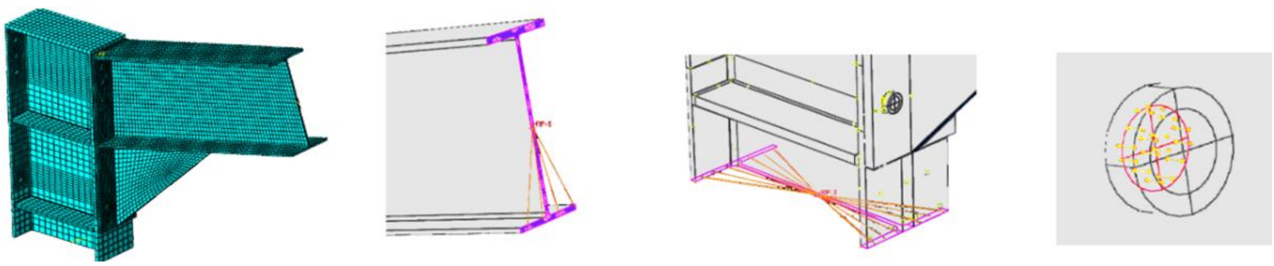

(a) Mesh distribution overview (b) Surface for applied displacement (c) Rigid support at column base (d) Surface for bold preload

Fig. 13 Configuration of FE model for eaves joint types

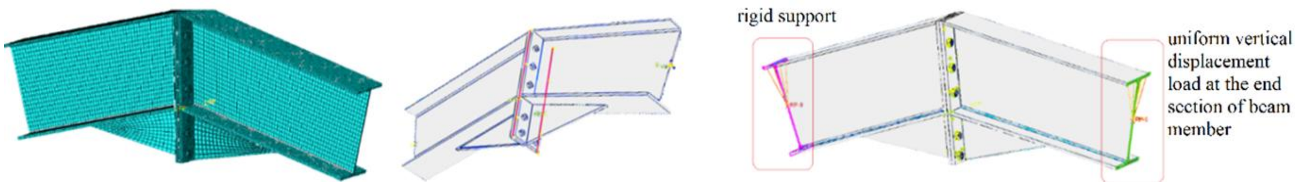


(a) Mesh distribution (b) Lateral restrains (c) Boundary condition and loading

Fig. 14 Configuration of FE model for apex joint types

A higher number of bolt row at the tension zone improves moment capacity of the joint by greater energy dissipation to the column flange under tension and the end plate. Localized yielding of column flange near the bolts at the tension zone was observed for joint type C1, C2 and C3. No sign of prying was noted. By comparing the same joints under moment reversal, the addition of an end-plate rib stiffener at the tension zone improves stress mobilization between the beam and column members, which explains the higher rotational stiffness and moment capacity of the said joints under negative moment.

### *6.2 Moment-rotation behaviour*

Fig. 20 and Table 5 show the $M$-Φ behaviours for all six joint configurations. Note that a stronger joint performance was clearly observed when the extended stiffened end-plate end come into tension instead of the flush end-plate end.

Type C1 model achieved 58% more moment capacity under positive bending than under negative bending (153.2 kNm for specimen C1 under positive moment and 242 kNm under negative moment). The difference was reduced to 29% when the number of bolt rows in the tension zone increases to 3 (Type C3). For all Type D specimens, the same trend was observed. The initial rotation stiffness for Type C1 model is 292% higher under positive bending than under negative bending. The value was reduced to 160% higher for specimen C3.

The calculation of lever arm for the studied joint type is taken as the vertical distance between the column-flange-to-end-plate contact zone (conservatively assumes as the zone adjacent to bottom beam flange for design purpose) and the horizontal pull-out force by bolt groups in the tension zone (Fig. 15). The longer lever arm is employed when the joint is under negative moment, which allows greater rotational stiffness and moment resistance than when under positive moment. By comparing Type C2+ve and C3+ve, the rotational stiffness increased further by another 122% but the moment resistance increased merely by 1%.

### *6.3 Effect of bolt group*

The influence in the quantity of tension bolts on the behaviour of the considered joint is studied in this section. In terms of initial rotational stiffness, the addition of a second bolt row in the tension zone in Type C2 joint has improved the rotational stiffness by 48% when compared with only one bolt row in the tension zone in Type C1 joint, while a third additional bolt row in Type C3 joint has improved the stiffness by a further 23% when compared with Type C2.This is due to the improvement in stress transfer between the flange and the web when more bolt rows were employed in the tension zone. Similar results were observed for Type D joints, with 203% increases in rotational stiffness by increasing from one bolt row (Type D1 joint) to two bolt rows (Type D2 joint), and a further 47% to three bolt rows (Type D3). In terms of the moment resistance, There is an 20 to 22% increases from Type C1 to Type C2 but merely 1% from Type C2 to Type C3, a similar trend is observed where a 22% increase is observed between Type D1 and Type D2, and yet a significantly less of 9% is observed between Type D2 and Type D3. This observation can conclude that, in terms of moment resistance, Type C1 and D1 have more to be benefitted from a second bolt row compared to a third bolt row as two bolt rows have twice the stress cone area than with one bolt row

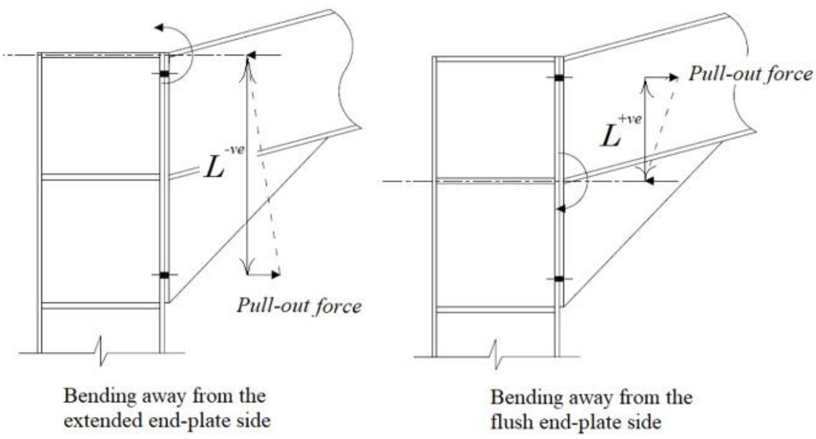


Fig. 15 Design assumptions of lever arm calculation for Type C1 joint

(Type C1), but three bolt rows (Type C3) have one third the stress cone area than with two bolt rows (Type C2). The

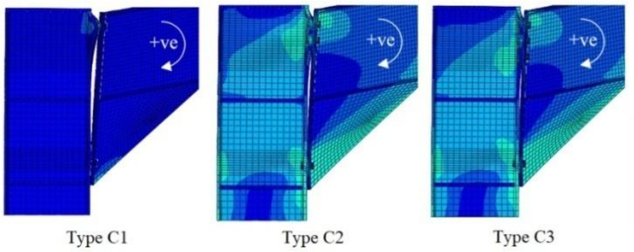


Fig. 16 Joint failure by column flange yielding under positive moment

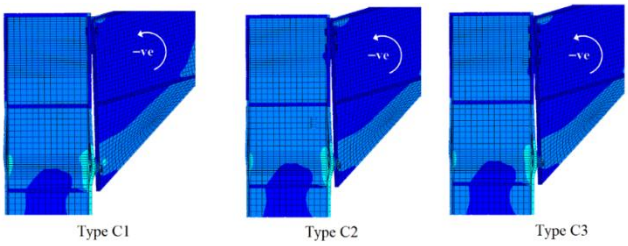


Fig. 17 Joint failure by column flange yielding under negative moment

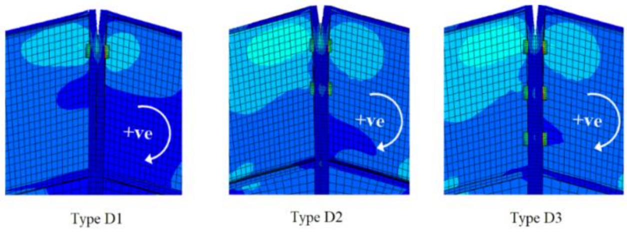


Fig. 18 Joint failure by end plate yielding under positive moment

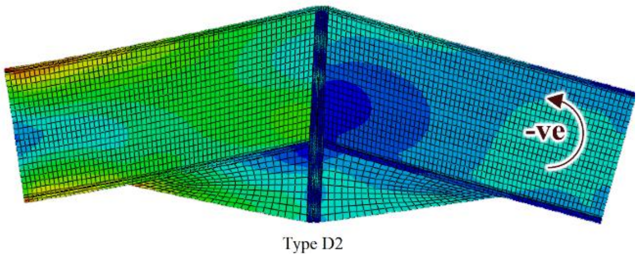


*Note: The deformation pictures of the two remaining Type D joints under are not shown in this paper due to visual identity to Type D2

Fig. 19 Joint failure by end plate buckling under negative moment*

Table 5 Joint assessment based on Eurocode-3 classification

| Joint No. | Moment direction | Joint stiffness class | Joint strength class | $M_{j,Rd}$ (KN.m) | $S_{j,ini}$ (MN.m/rad) | $\Phi_c$ (mrad) | Failure limit state (initial yielding) |
|---|---|---|---|---|---|---|---|
| C1 | +ve | Semi-rigid | Partial | 153.2 | 75.5 (13.5 $EI/L$) | 19.5 | Column flange yielding |
| | –ve | Nominally rigid | Full | 242 | 220.6 (36.3 $EI/L$) | 1056.6 | Member yielding failure [a] |
| C2 | +ve | Semi-rigid | Partial | 183.2 | 112.1 (20.0 $EI/L$) | 47.2 | Column flange yielding |
| | –ve | Nominally rigid | Full | 242 | 220.6 (36.3 $EI/L$) | 1056.6 | Member yielding failure [a] |
| C3 | +ve | Semi-rigid | Partial | 186.3 | 137.5 (24.5 $EI/L$) | 47.3 | Column flange yielding |
| | –ve | Nominally rigid | Full | 242 | 220.4 (39.2 $EI/L$) | 1052.5 | Member yielding failure [a] |
| D1 | +ve | Semi-rigid | Partial | 158.5 | 22.8 (4.07 $EI/L$) | 43.5 | End-plate yielding |
| | –ve | Nominally rigid | Full | 242 | 238.6 (42.6 $EI/L$) | 1444.2 | Beam flange yielding |
| D2 | +ve | Semi-rigid | Partial | 193.9 | 46.422.8 (8.29 $EI/L$) | 63.3 | End-plate yielding |
| | –ve | Nominally rigid | Full | 242 | 239.6 (42.6 $EI/L$) | 1405.7 | Beam flange yielding |
| D3 | +ve | Semi-rigid | Partial | 209.2 | 68.4 (12.2 $EI/L$) | 83.9 | End-plate yielding |
| | –ve | Nominally rigid | Full | 242 | 239.8 (42.7 $EI/L$) | 1405.7 | Beam flange yielding |

[a] Member yielding is a failure limit state to describe the case of a strong-connection weak-member scenario where a member yields earlier than any components of a connection

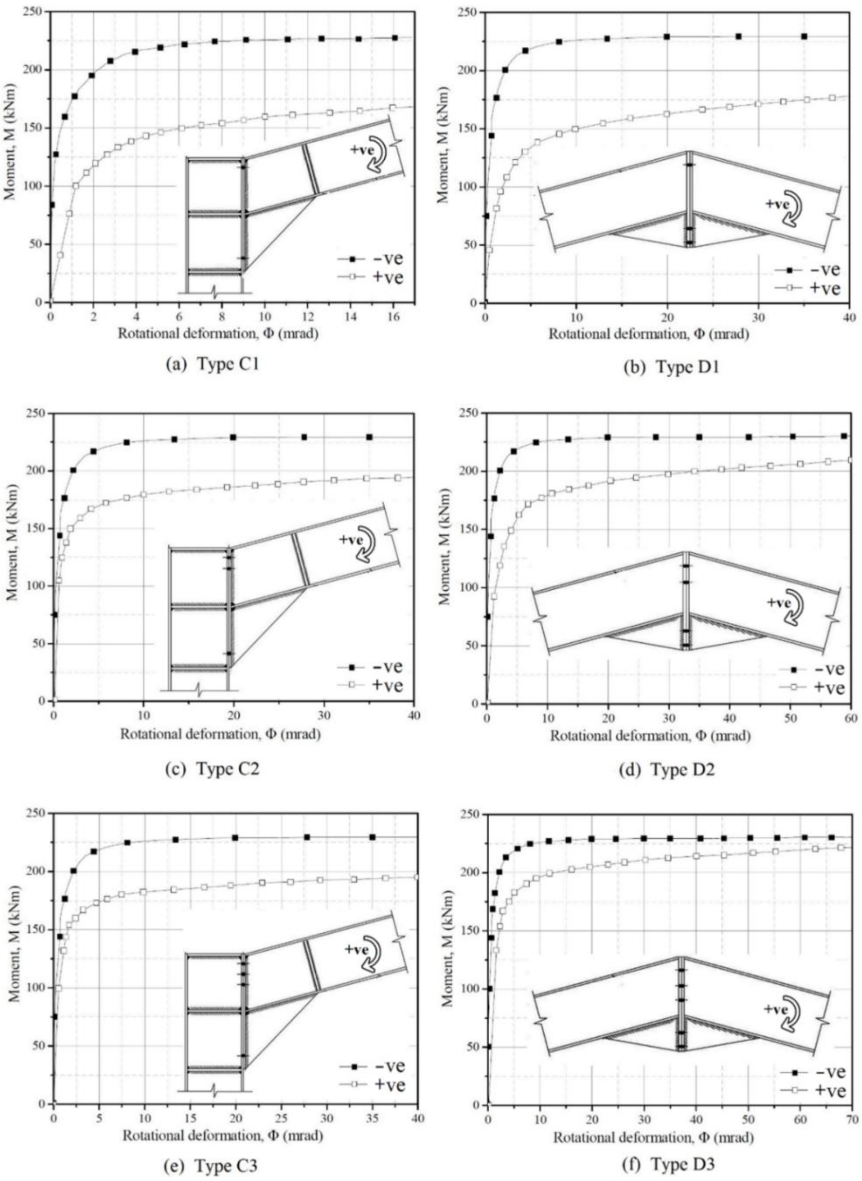


Fig. 20 Moment-Rotation relationships of the six asymmetrical joints

second reason may be due to the reduction in lever arm between the third bolt row compared to the second bolt row which reduces the effectiveness of the third bolt row in providing both stiffness and resistance.

### *6.4 Effect of an end-plate rib stiffener*

The addition of an end-plate rib stiffener increases the joint stiffness by minimizing the deformation in the end-plate, which improves the end-plate flexural resistance. In Fig. 15, the lever arm is conservatively assumed as such in a typical design practice, where L-ve is the lever arm for negative bending and L+ve for positive bending. As expected, all Type C joints exhibit higher stiffness under negative bending when L-ve was used. Furthermore, under negative bending, first yielding occurred nearly simultaneously to the beam and column flanges outside the connection zone, with the column flange detecting the highest strain within the connection zone which is only 1.1% at the instance of first yielding in the members. This shows that a minimal amount of bolt row is required for achieving full-strength rigid joint when the bending moment is applied away from the extended end-plate end. Conversely, a full-strength nominally rigid joint cannot be achieved even if a maximum number of tension bolt rows is used for the same joint under positive bending due to the lack of web rib stiffener on the tension side of the joint.

## 7. Conclusion of FEM results

Table 5 summarizes the joint performance characteristics according to Eurocode-3 classification and Fig. 20 shows the $M$-Φ relationships of the six asymmetrical joints under positive or negative bending moment. The six joint models exhibit higher bending resistance as well as rotational stiffness when their extended ends are in tension by negative moment. Since the extended end is often more

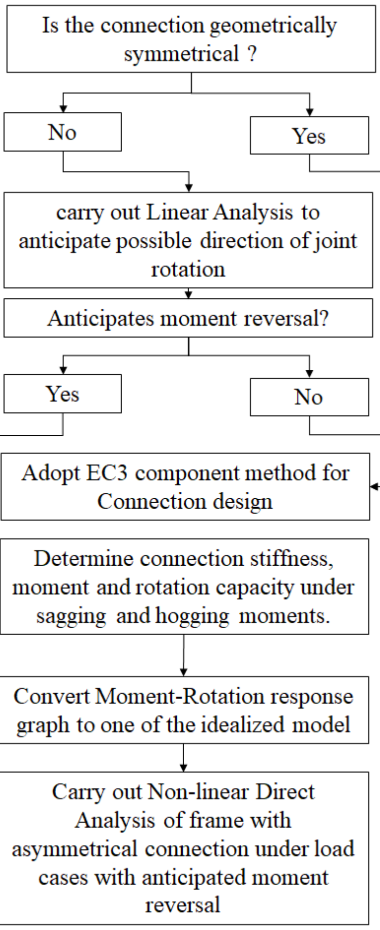


Fig. 21 Design flow chart of frame with asymmetrical joint by direct analysis

effective in stress mobilization between the joint components compared to the flushed end, a typical haunch joint is often not well utilized in positive bending due to the weaker flush end in control of the joint overall strength.

## 8. Plastic direct analysis of frames with semi-rigid joint

### 8.1 Description of the design work flow

An overview of the proposed design of a frame under asymmetrical semi-rigid joints developed for this paper is shown in Fig. 21 above

### 8.2 Modelling of asymmetrical M-θ response curve of semi-rigid joint

The model characteristic is based on the Eurocode-3 traditional criteria of a joint, which are bending strength, stiffness, and ductility. Effort is spent on the integration of negative-positive joint moment curvature onto the recent curved-quartic-function element with end-spring which models the effects of semi-rigid joints and material yielding under large deflection effects with the one-element-per-member model.

### 8.3 Non-linear analysis of Vogel gable frames with asymmetrical joints

To investigate the structural response of frame under asymmetrical joints, the models developed from this paper were applied to the benchmarked examples as Vogel gable frame and Vogel six storey frame (Vogel 1985). The material and geometrical properties of the frames and their constituting members are available in the original publication.

For verification purpose of the modelling technique, the load-displacement curve of the Vogel gable frame is computed by $4^{th}$ order polynomial function of present study and is compared with Vogel plastic zone theory (Vogel 1985) with agreeable outcome shown in Fig. 22.

The load-displacement curves of Type 1 frame (Fig. 23) and Type 2 frame (Fig. 24) are computed by the $4^{th}$ order polynomial element and are shown in Figs. 25-26 respectively. These two figures show that the structural

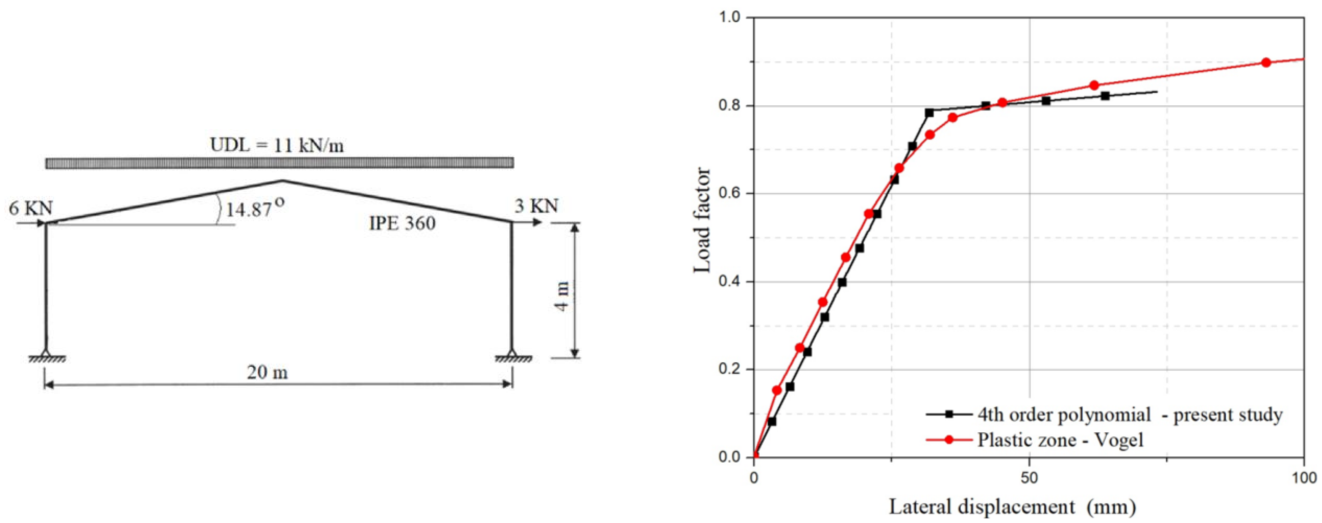


(a) (b)

Fig. 22 (a) Configuration of Vogel gable frame; (b) comparison of load–deflection curve with Vogel's plastic zone theory (Vogel 1985)

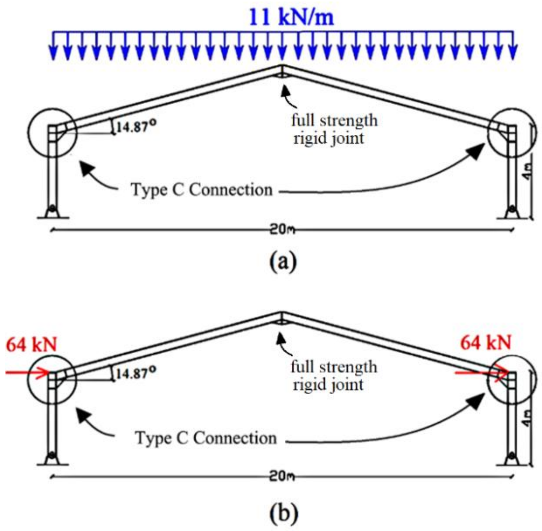


Fig. 23 Loading and dimension details of Type 1 Frame (a) Load Case 1: gravity load; (b) Load Case2: Lateral wind load

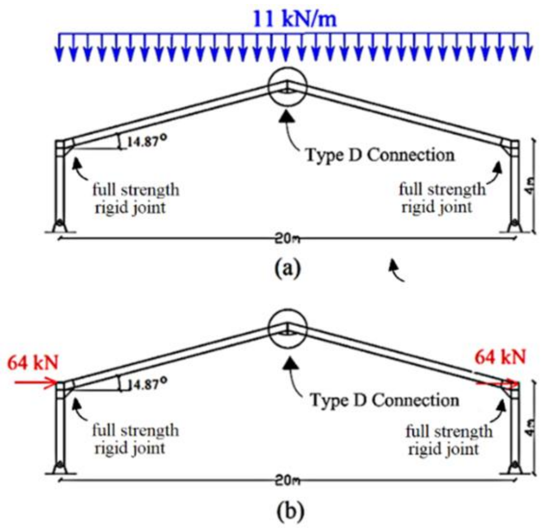


Fig. 24 Loading and dimension details of Type 2 Frame (a) Load Case 1: Gravity Load; (b) Load Case2: Lateral Wind Load

stiffness and the load capacity of each frame were affected by asymmetrical $M$-$\theta$ behaviour of Type C joints (eave joint) for Load Case 2 where negative moment exist at the eave joint. In particular, the asymmetry of joints for Type 1 and Type 2 frames under Load Case 1 (Gravity Load only) has no effect on the load-displacement graph because all beam-column joints of the frame has similar performance under positive moment. As shown in Table 6, load capacity of Type 1 frame is found to be more susceptible to joint asymmetry than Type 2 frame, this is explained by the fact that an apex joint from the gable frame is not under predominant bending as opposed to the eave joints and therefore it is less affected by the bending performance of joint. From Fig. 27 to 29, significant increases in load-carrying capacities of Type 1 frames can be observed by adopting the proposed design approach for asymmetrical

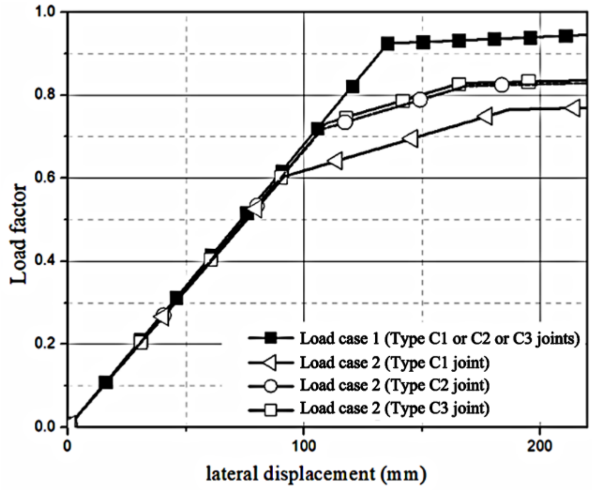


Fig. 25 Structural responses of Type 1 frame under Load case 1 and 2

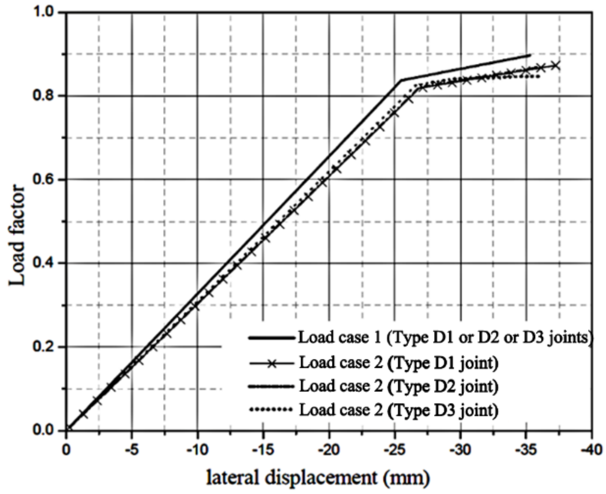


Fig. 26 Structural responses of Type 2 frame under Load case 1 and 2

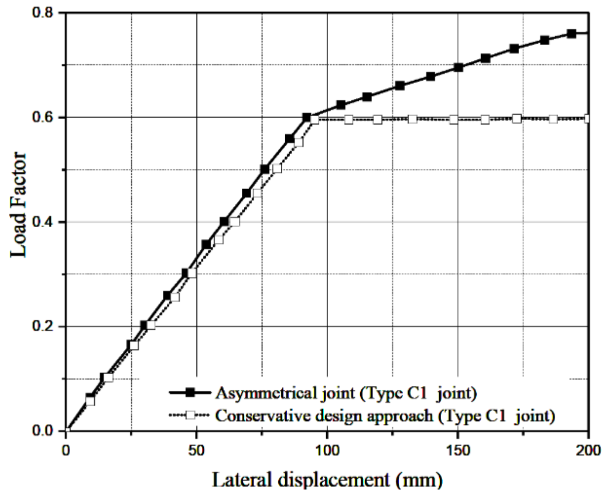


Fig. 27 Structural responses of Type 2 frame with proposed asymmetrical joint design method against the conservative design approach for Type C1 joint under Load case 2 (lateral wind load only)

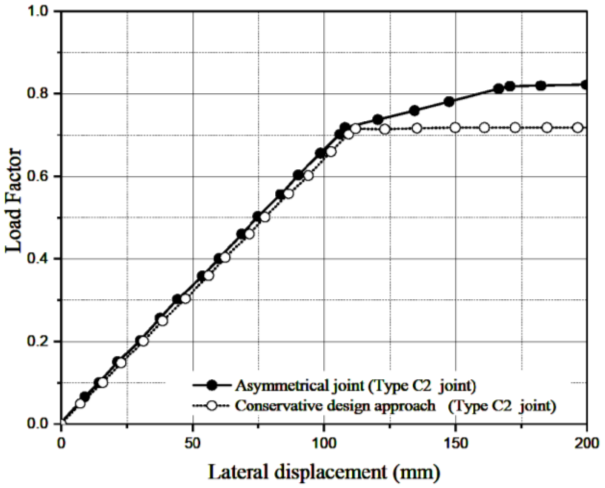


Fig. 28 Structural responses of Type 2 frame with proposed joint design assumption versus the conservative design approach for Type C2 joint under Load case 2 (lateral wind load only)

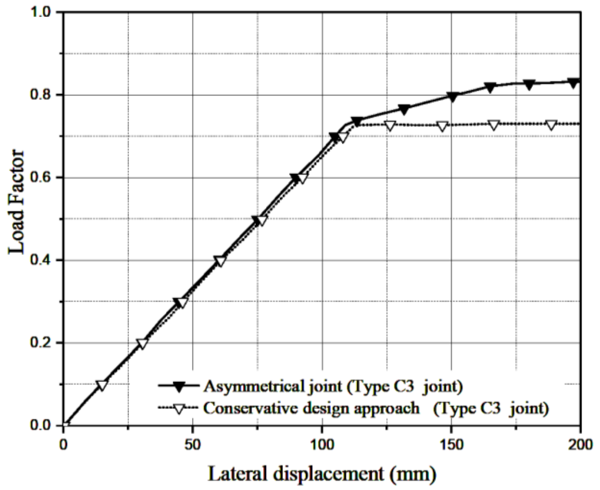


Fig. 29 Structural responses of Type 2 frame with proposed asymmetrical joint design assumption against the conservative design approach for Type C3 joint under Load case 2 (lateral wind load only)

joints instead of the conservative design approach where the weaker bending direction is assumed to represent stiffness and strength for the joint under either positive or negative bending. This demonstrated great potential in material economy for adopting such design method. More importantly, the method provides a more accurate failure mode assessment and bending moment profile which would affect the corresponding member design considerably. From the results of Table 6, the collapse load of the gable frame is shown to be reduced by 35%, 22% and 21% respectively if joint type C1, C2 and C3 are adopted instead of a nominally rigid joint. However, a minor reduction of 2% or less is observed for the apex joint types D1, D2 and D3 which are predominantly stressed axially.

Table 6 Summary of normalized Load Factor for Vogel's gable frame with asymmetrical joints under Load Case 2 (Lateral Wind Load only))

| Adopted joint type | Normalised load factor, $\lambda_u$ |
|---|---|
| Nominally rigid | 1 |
| Type C1 (Type 1 frame) | 0.65 |
| Type C2 (Type 1 frame) | 0.78 |
| Type C3 (Type 1 frame) | 0.79 |
| Type D1 (Type 2 frame) | 0.98 |
| Type D2 (Type 2 frame) | 0.98 |
| Type D3 (Type 2 frame) | 0.99 |

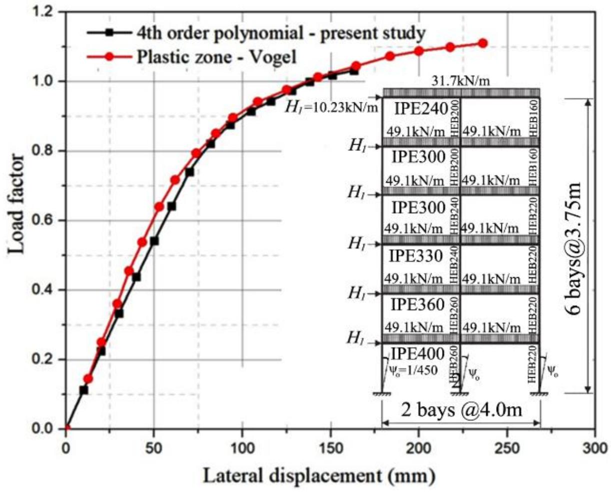


Fig. 30 Comparison of load–deflection curves for Vogel's six-storey frame under benchmark Load Case

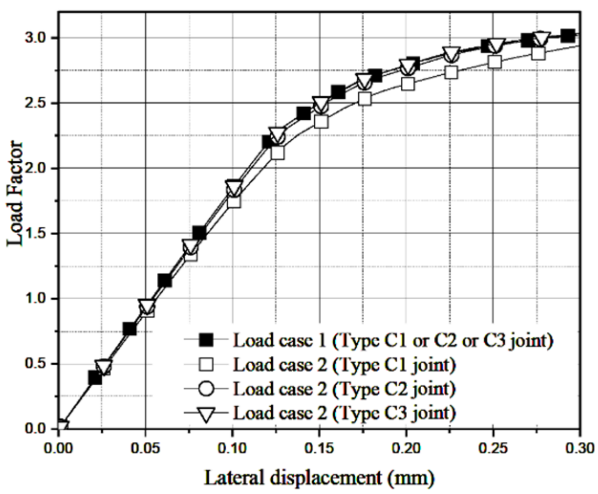


Fig. 31 Structural responses of Vogel's six storey frame with type A and type C joints

*Note: Negative moment is generated by Load Case 1: (Gravity Load only), And positive moment by Load Case 2: (Lateral Wind Load only))

### *8.4 Non-linear analysis of Vogel six-storey frames with asymmetrical joints*

The load-displacement curve of the Vogel six-storey frame shown in Fig. 30 is computed by 4$^{th}$ order polynomial function of present study and yields agreeable outcome with the Vogel's plastic zone theory (Vogel 1985). In the present study, all the structural members would adopt IPE360 for the study of its structural response with Type C joints which adopts section IPE360. This example serves to highlights the effect of joint asymmetry on the frame behaviour and the results are shown in Fig. 31.

The design load capacity factor ($\lambda_u$) of the Vogel six storey frame (Vogel 1985) is determined based on "the first plastic-hinge design", where the minimum load factor required for the formation of the first plastic hinge is used. The results are summarised in Table 7. The load-displacement result plotted in Fig. 31 illustrates that the effect of Type 3 joint asymmetry on the structural responses of the six storey frame was not as prominent as our previous example, i.e., the variation in load factor between different Type C joints was all within 8% as shown in Table 7, as opposed to 35% for the Vogel gable frame model earlier in this study (see Table 6).

By the bending moment diagram illustrated in Fig. 32 below, the frame model was still structurally stable after the formation of the three plastic hinges across all three columns at the ground storey, resulting in a pinned based structure with moment resisting beam-column joints which was still structurally stable. This illustrates that since the present frame derives its lateral stiffness from both its beam-column joints and its rigid column support, the asymmetry of the beam-column joint has less effect to the overall load-deflection shape of the frame compared to the gable frame with pinned support in earlier chapter. Briefly speaking for the frame failure mode, the frame reached its collapse load when more plastic hinges were formed at the columns of the second storey, which caused in-plane sway instability (a failure mechanism). Fig. 32 below, which illustrates the bending moment diagram of the six storey frame under Load Case 2 (Lateral Wind Load only) would result in one end of each beam to be subjected with positive bending and the opposite end with negative bending.

It is illustrated that the possibility of a moment reversal to a structure with asymmetrical bolted joints such as those studied in this paper could have a significant impact to the structure load-carrying capacity of structures, hence the moment-rotation relationships of asymmetrical bolted joints should be modelled in a Direct Analysis for safe structural design and analysis.

Table 7 Summary of normalized Load Factor for Vogel's six-storey frame with asymmetrical joints under Load Case2 (Lateral Wind Load only)

| Joint type | Normalised load factor, $\lambda_u$ |
|---|---|
| Nominally rigid | 1 |
| C1 | 0.92 |
| C2 | 0.95 |
| C3 | 0.96 |

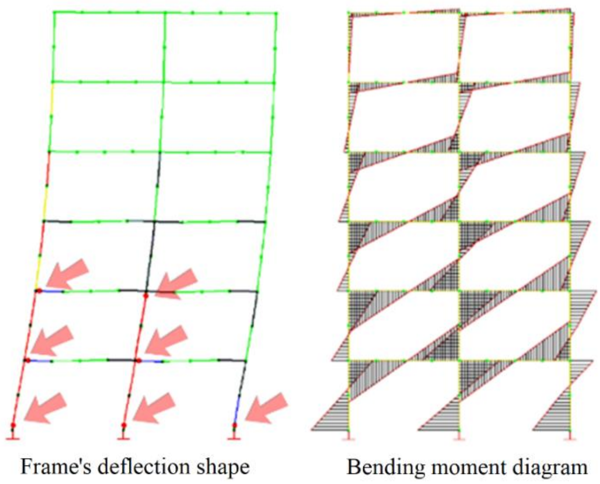


Fig. 32 At the stage of collapse (collapse load factor = 3) under Load Case 2 (Lateral Wind Load only)

## 9. Conclusions

A robust direct analysis of semi-rigid frames allowing for asymmetrical *M-θ* behaviour is presented and this consideration appears to have not been included in previous research work, but unavoidable in typical joint details for some common steel structures. This paper further presents an investigation on its influence to the non-linear structural response of a Vogel gabled frame and six-storey frame. The *M-θ* characteristics for a series of apex and eaves joints were evaluated by FEM and adopted in frame analysis and design of the two frame types. It was found that the *M-θ* characteristics of the six studied joints are mostly asymmetrical as expected and are classified from full-strength rigid by positive moment to partial-strength semi-rigid by negative moment. When under Load Case 2 (Lateral Wind Load only), the associated non-linear structural analysis reveals the effect of asymmetrical behaviours to be significant with a reduction in loading capacity of up to 35% for the Vogel gable frame and 8% for the Vogel six storey frame. FEM result also shows that the number of bolt rows in tension affects the initial rotational stiffness of the joint considerably but not always the case for the moment resistance. In order to avoid unsafe and under-design of structures, asymmetrical behaviour in joints should be considered.

## Acknowledgments

This study would not have been possible without the corporation and support extended by Wolee Steel Co. Ltd. The authors are also grateful for the dedicated technical staffs at the two testing facilities at the University of Hong Kong and the Hong Kong Polytechnic University where tests were conducted.

## References

ABAQUS Standard User's Manual (2014), Version 6.14, Hibbitt, Karlsson & Sorensen, Inc., RI, USA.

AISC (2010), Specification for structural steel buildings; American Institute of Steel Construction, Chicago, IL, USA.
Bai, L., Jiang, F. and Wang Z. (2016), "Effects of semi-rigid joints on reliability of steel frames under three-states", *J. Huazhong Univ. Sci. Technol.* (Nature Science Edition), **44**(1).
Bell, W.G., Chesson, E.J. and Munse, W.H. (1958), *Static Tests of Standard Riveted and Bolted Beam-to-Column Joints*, University of Illinois, Engineering Experiment Station, Urban, IL, USA.
Chen, W.F. and Kishi, N. (1989), "Semi rigid steel beam-to-column connections: Data base and modeling", *J. Struct. Eng.*, **115**(1), 105-119.
Daryan, A.S., Sadri, M., Saberi, H., Saberi, V. and Moghadas, A.B. (2012), "Behaviour of semi-rigid joints and semi-rigid frames", *Struct. Des. Tall Special Build.*, **23**(3), 210-238.
Davison, J.B., Kirby, P.A. and Nethercot, D.A. (1987), "Rotational stiffness characteristics of steel beam-to-column connections", *J. Constr. Steel Res.*, **8**, 17-54.
Eurocode 3 (2005), Design of Steel Structure. Part 1.8: Design of Joints; European Committee for Standardization: Brussels, Belgium.
Johnson, N.D. and Walpole, W.R. (1981), "Bolted End Plate Beam to Column Connections Under Earthquake Type Loading", Research Report 81-7; Department of Civil Engineering, University of Canterbury, Christchurch, New Zealand.
Kim, S.E., Kim, M.K. and Chen, W.F. (2000), "Improved refined plastic hinge analysis accounting for strain reversal", *Eng. Struct.*, **22**(1), 15-25. DOI: 10.1016/S0141-0296(98)00079-0
Kwak, H.G. and Kim, S.P. (2002), "Nonlinear analysis of RC beams based on moment–curvature relation", *Comput. Struct.*, **80**, 615-628.
Li, Z.S., Li, X.M., Zheng, X.W. and Zhang, K. (2014), "Experimental study and numerical investigation on hysteretic behaviour of T-stub semi-rigid beam-to-column joints", *J. Build. Struct.*, **35**(7), 61-68.
Liew, J.Y., White, D.W. and Chen, W.F. (1993), "Second-Order Refined Plastic-Hinge Analysis for Frame Design. Part 1", *J. Struct. Eng.*, **119**(11).
Liu, S.W., Bai, R. and Chan, S.L. (2016a), "Dynamic time-history elastic analysis of steel frames using one element per member", *Struct. J.*, 8(2), 300-309.
Liu, J., Peng, P. and Liu, D.L. (2016b), "Neural Network Model of Moment-rotation Relation in Semi-rigid Beam-column Joints Considering Floor Stiffness", *J. Architect. Civil Eng.*, **33**(1).
Meek, J.L. and Tan, H.S. (1984), "Geometrically nonlinear analysis of space frames by an incremental-iterative technique", *Comput. Methods Appl. Mech. Eng.*, **47**, 261-282.
Moore, D.B., Nethercot, D.A. and Kirby, P.A. (1993), "Testing steel frames at full scale", *Struct. Engr.*, **71**, 418-427.
Nassani, D.E., Chikho, A.H. and Akgonen, A.I. (2017), "Semi-rigidity of cap plate and extended end plate connections", *Steel Compos. Struct., Int. J.*, **23**(5), 493-499.
Nguyen, P.C. and Kim, S.E. (2016), "Advanced analysis for planar steel frames with semi-rigid connections using plastic-zone method", *Steel Compos. Struct., Int. J.*, **21**(5), 1121-1144.
Ostrander, J.R. (1970), "An Experimental Investigation of End-Plate Joints", Master's Thesis; University of Saskatchewan, Saskatoon, SK, Candada.
Rafiee, A., Talatahari, S. and Hadidi, A. (2013), "Optimum design of steel frames with semi-rigid connections using Big Bang-Big Crunch method", *Steel Compos. Struct., Int. J.*, **14**(5), 431-451.
Rathbun, J.C. (1936), "Elastic properties of riveted connections", *Transact. Am. Soc. Civil Engr.*, **101**(1), 524-563.
Sagiroglu, M. and Aydın, A.C. (2013), "Design and Analysis of Steel Space Frame with Semi-Rigid Beam-to-Column Joints Using Stiffness Method", *Proceedings of the 10th Pacific Structural Steel Conference*, Singapore.
Sagiroglu, M., Aydın, A.C. and Cuneyt, A. (2015), "Design and analysis of non-linear space frames with semi-rigid connections", *Steel Compos. Struct., Int. J.*, **18**(6), 1405-1421.
SCI P358 (2011), Joints in Steel Construction: Simple Joints to Eurocode 3: 2014 Re-print ed. Ascot, UK: The Steel Construction Institute & The British Constructional Steelwork Association Limited.
Sommer, W.H. (1969), "Behaviour of welded header plate joints", Master's Thesis; University of Toronto, ON, Canada.
Valipour, H.R. and Bradford, M.A. (2013), "Nonlinear P-Δ analysis of steel frames with semi-rigid connections", *Steel Compos. Struct., Int. J.*, **14**(1), 1-20.
Vogel, U. (1985), "Calibrating frames", *Stahlbau*, **54**, 295-301.
Wilson, W.M. and Moore, H.F. (1917), "Tests to determine the rigidity of riveted joints of steel structures", Bulletin No. 104; Engineering Experiment Station, University of Illinois, Urbana, IL, USA.
Young, C.R. and Jackson, K.B. (2011), "The relative rigidity of welded and riveted connections", *Can. J. Res.*, **11**(1), 62-100.
Yu, C.H., Liew, J.Y., Shanmugam, N.E. and Ng, Y.H. (1998), "Collapse behaviour of sway frames with end-plate connections", *J. Constr. Steel Res.*, **48**(2-3), 61-214.

*DL*